Disintegration of the Deuteron by Tagged, Linearly-Polarized Photons: Sensitivity of the Differential Cross Sections

V. P. Likhachev[*], M. N. Martins, Yu. A. Kasatkin[†], M. T. F. da Cruz, J. D. T. Arruda-Neto, R. Guarino, V. B. Shostak[‡]

Laboratório do Acelerador Linear

Instituto de Física da Universidade de São Paulo

Rua do Matão, Travessa R 187

05508–900 São Paulo, SP, Brasil

Received March 20, 1997

We present results of theoretical calculations together with simulations for some observables of the reaction $\overrightarrow{\gamma} d \rightarrow np$ at energies close to the threshold. This approach allows the selection of the set of observables and the best kinematical conditions in order to probe different potentials. The simulations used the parameters of the forthcoming São Paulo Microtron accelerator and photon tagging facilities.

I. Introduction

The photodisintegration of the deuteron is a powerful tool for studying the nucleon-nucleon interaction, helping to probe the various NN potentials. The advantage of this experiment is that we combine the well-known electromagnetic interaction with the study of the simplest nuclear aggregate. The disintegration of the deuteron is usually a test case for new experimental techniques, also bringing up more information about the strong interaction.

The interpretation of low-energy breakup data presents problems when one tries to make use of realistic potentials, as those associated to (a) the choice of observables sensitive to the NN-force properties and their description; (b) the introduction of non-nucleonic degrees of freedom, like meson-exchange currents (MEC); and (c) the isobar configurations and relativistic corrections to the one- and two-body currents. Effects like final-state interaction (FSI) must also be taken into account [1].

The near-threshold region is particularly noticeable, due to simplifications on both theoretical and experimental aspects, as (a) the presence of a dominant multipole (usually $E1$ or $M1$), with negligible contributions from the others at the entrance channel; each multipole takes few partial waves in the exit channel; and (b) the absence of background from other channels or competing reactions. All this simplifies the interpretation of low-energy data.

The use of polarized tagged photons is of particular interest, because the polarization observables contain interference terms between reaction amplitudes and are sensitive to small amplitudes belonging to contributions of non-nucleonic degrees of freedom. Although the latter are generally small, this is compensated by the high experimental accuracy attainable in this energy range. Besides, FSI effects are strong close to the threshold

[*] On leave from Kharkov Institute of Physics and Technology, Ukraine.
[†] Kharkov Institute of Physics and Technology, Ukraine.
[‡] Kiev Institute of Nuclear Physics, Ukraine.

and, thus, convenient to be studied.

This work presents an analysis of the sensitivity of differential cross sections for different theoretical predictions in the photon low-energy region. Predictions of different calculations are analyzed with the expected experimental results obtained from Monte Carlo simulation, including an analysis of the experimental uncertainties expected for the experimental conditions of the São Paulo Microtron Accelerator and photon tagging facilities.

II. General definitions

The differential cross section of the reaction $\overrightarrow{\gamma} d \rightarrow np$ (see Fig.1.a) can be expressed in terms of the helicity amplitudes [2] for γ-quanta, with any polarization, incident on a non-polarized target, and in the center of mass system (CM), as follows

$$\frac{d\sigma}{d\Omega} = \frac{1}{(8\pi W)^2} \frac{\mid \overrightarrow{p} \mid}{\mid \overrightarrow{K} \mid} Sp\{R\} \tag{1}$$

where

$$Sp\{R\} = \sum_{\{\lambda\}} T^{\lambda_\gamma,\lambda_d}_{\lambda_p,\lambda_n} \rho_{\lambda_\gamma,\lambda'_\gamma} T^{*\lambda'_\gamma,\lambda_d}_{\lambda_p,\lambda_n}, \tag{2}$$

$T^{\lambda_\gamma,\lambda_d}_{\lambda_p,\lambda_n}(W, \cos\theta_p)$ is the CM helicity amplitude; λ_q, $q = \gamma, d, p, n$, are the helicities of the photon, deuteron, proton and neutron, respectively; $W = D_0 + K_0 = 2E_0$ is the energy of the pn pair, and θ_p is the angle between the momenta of the photon and the outgoing proton (see Fig.1.b). In the case of a coincidence experiment, $\Delta\Omega$ is the solid angle subtended by the detector pair, according to the reaction kinematics; $\rho_{\lambda_\gamma,\lambda'_\gamma}$ is the polarization density matrix of the photon [3]. For the case of a completely linearly polarized photon, their elements are

$$\begin{aligned} \rho_{1,1} &= \rho_{-1,-1} = \frac{1}{2}, \\ \rho_{1,-1} &= -\frac{1}{2} e^{-2i\phi}, \\ \rho_{-1,1} &= \rho^*_{1,-1}, \end{aligned} \tag{3}$$

where ϕ is the angle between the polarization vector of the photon and the x axis (see Fig.1.b). Using (2) and (3), the cross section can be written, in the case of partial polarization, as:

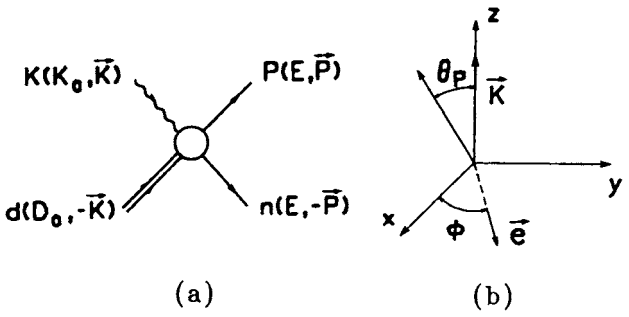

Figure 1. General notation.

$$\frac{d\sigma}{d\Omega}(\theta, \phi, E_\gamma) = \frac{d\sigma_0}{d\Omega}(\theta, E_\gamma) + P_\gamma \frac{d\sigma_1}{d\Omega}(\theta, E_\gamma) \cos(2\phi), \tag{4}$$

where

$$\frac{d\sigma_0}{d\Omega}(\theta, E_\gamma) = \frac{1}{2}\left(\frac{d\sigma_\parallel}{d\Omega}(\theta, E_\gamma) + \frac{d\sigma_\perp}{d\Omega}(\theta, E_\gamma)\right). \tag{5}$$

Here we have used the following notation for the differential cross sections

$$\frac{d\sigma_{\{\parallel\}}}{d\Omega} = \frac{d\sigma}{d\Omega}(\phi = \left\{ \begin{matrix} 0 \\ \frac{\pi}{2} \end{matrix} \right\}), \tag{6}$$

where the upper (lower) subscript on the left corresponds to the upper (lower) choice of ϕ on the right hand side. P_γ is the degree of linear polarization of the photon and $d\sigma_1/d\Omega$ characterizes the azimuthal asymmetry. We can define the azimuthal cross section asymmetry, $\Sigma(\theta, E_\gamma)$, as

$$\Sigma(\theta, E_\gamma) = \left(\frac{d\sigma_1/d\Omega}{d\sigma_0/d\Omega}\right) = \frac{1}{P_\gamma} \frac{(d\sigma_\parallel/d\Omega) - (d\sigma_\perp/d\Omega)}{(d\sigma_\parallel/d\Omega) + (d\sigma_\perp/d\Omega)}. \tag{7}$$

The differential cross section can then be written as

$$\frac{d\sigma}{d\Omega}(\theta,\phi,E_\gamma) = \frac{d\sigma_0}{d\Omega}(\theta,E_\gamma)\left[1 + P_\gamma\Sigma(\theta,E_\gamma)\cos(2\phi)\right]. \tag{8}$$

For complete linear polarization, $P_\gamma = 1$, and with a convenient choice of directions, the differential cross sections can be written as

$$\frac{d\sigma_{\parallel,\perp}}{d\Omega}(\theta,E_\gamma) = \frac{d\sigma_0}{d\Omega}(\theta,E_\gamma)\left[1 \pm \Sigma(\theta,E_\gamma)\right], \tag{9}$$

where the sign $+(-)$ on the right corresponds to $\parallel$ ($\perp$).

The statistical uncertainties of the differential cross sections are

$$\Delta\left(\frac{d\sigma_{\parallel,\perp}}{d\Omega}\right) = \left\{\left[\Delta\left(\frac{d\sigma_0}{d\Omega}\right)\right]^2(1\pm\Sigma)^2 + \left(\frac{d\sigma_0}{d\Omega}\right)^2(\Delta\Sigma)^2\right\}^{\frac{1}{2}}, \tag{10}$$

where $\Delta(d\sigma_0/d\Omega)$ and $\Delta\Sigma$ are the statistical uncertainties of the $d\sigma_0/d\Omega$ cross section and of the Σ-asymmetry, respectively. The uncertainty of the Σ-asymmetry is

$$\Delta\Sigma = \frac{1}{2P_\gamma N_0}\left\{\left(\Delta N_\parallel\right)^2 + \left(\Delta N_\perp\right)^2 + \left(N_\parallel - N_\perp\right)^2\left[\left(\frac{\Delta P_\gamma}{P_\gamma}\right)^2 + \left(\frac{\Delta N_0}{N_0}\right)^2\right]\right\}^{\frac{1}{2}}, \tag{11}$$

where $\Delta P_\gamma/P_\gamma$ is the relative uncertainty of the degree of linear polarization and $N_{0,\parallel,\perp}$ and $\Delta N_{0,\parallel,\perp}$ are the measured experimental yields and their uncertainties for each polarization situation, with

$$\Delta N_{0,\parallel,\perp} = \left[\left(1 + R_{0,\parallel,\perp}\right)N_{0,\parallel,\perp}\right]^{\frac{1}{2}}, \tag{12}$$

where $R_{0,\parallel,\perp}$ is the ratio of the number of random to true coincidences, for each polarization situation.

The number of counts for one tagging energy interval (energy bin) can be evaluated by the following expression:

$$N_{0,\parallel,\perp} = \frac{d\sigma_0}{d\Omega}N_n N_\gamma^{tag} t\,(4\pi\epsilon)\left\{\begin{array}{c} 1 \\ 1+P_\gamma\Sigma \\ 1-P_\gamma\Sigma \end{array}\right\} \tag{13}$$

where N_n is the number of nuclei per cm^2 in the target, N_γ^{tag} is the number of photons per second per tagger channel, t is the acquisition time and ϵ is the absolute efficiency of the detector pair. The parameter $4\pi\epsilon$ includes the geometrical solid angle defined by the detectors at the target position and the intrinsic efficiency of the detectors. The absolute efficiency ϵ, determined by Monte Carlo simulation [4], corresponds to a weighted average of the intrinsic efficiency over the solid angle defined by the detector's surface. Since this is a coincidence experiment, the solid angle is actually a dynamic one, because its evaluation includes the kinematics of the reaction [4].

III. Theoretical Model

The theoretical analysis was carried out in the framework of a relativistic, gauge-invariant theory of the photo- and electrodisintegration of light nuclei. This approach was developed during the last few years [5, 6, 7, 8] and is based on quantum field theory with methods which allow to introduce nuclear structure, final-state interaction and MEC effects, although these last are present non-explicitly, via gauge-invariance constraints.

Fig. 2 shows two sets of diagrams used in the calculation. Set number I corresponds to the relativistic pole approximation. The last diagram takes MEC into account. The contact current does not have pole-type peculiarities, but must be taken into account in the pole approximation, because the contact amplitude is the one that provides nuclear current conservation for this set of diagrams.

Set number II is characterized by the nuclear vertex function $d \rightarrow pn$ and by the half off-shell T matrix of $pn \rightarrow pn$ scattering. Diagrams (5) and (6) correspond to the usual final-state interaction; loop diagrams (7) and (8) are necessary for current conservation, and account for both final-state interactions and meson-exchange currents.

FSI was taken into account through the $^1S_0$ resonance, its contribution to the amplitudes of the pn rescattering being calculated via a multipole expansion as

$$f_l = A_l \frac{e^{2i\delta_l} - 1}{2i}, \tag{14}$$

where

$$\delta_l = \delta_l^{background} + \delta_l^R, \tag{15}$$

with

$$\delta_l^R = \arctan\left[\frac{G_R}{2\left(M_R c^2 - W\right)}\right]. \tag{16}$$

The parameters of the resonance are $G_R c^2 = 300\ keV$, $M_R c^2 = m_p + m_n + I_R$, and $I_R c^2 = 67\ keV$. The background phase shift was calculated as in ref. [9]. The resonance forces, A_l, were calculated by the one-loop diagrams of Fig. 2 [5].

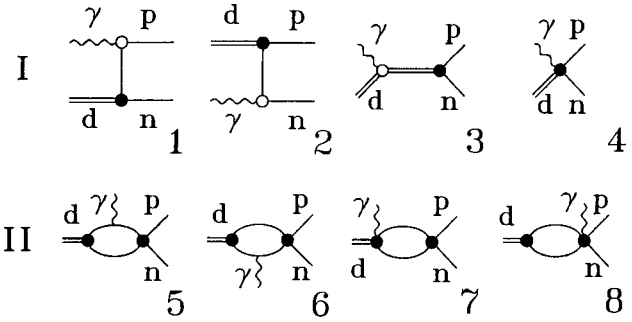

Figure 2. Two gauge invariant sets of diagrams used for the description of the deuteron photobreakup.

We have used two types of realistic deuteron wave functions: the first given by the Paris potential [10] (called DWF_1), and the other is the relativistic Gross' wave function [11] (DWF_2). They adequately describe not only the ground state properties, but also the elastic and quasielastic form factors.

IV. Results and discussion

One of the objectives of this paper is to find out the conditions where discrepancies, arising from different theoretical predictions, could be identified by experiment. In this section we first describe the experimental conditions that will be attained at the Linear Accelerator Laboratory, with the use of the São Paulo Microtron and the photon tagging facilities. Next, we present the theoretical calculations and Monte Carlo simulations, and describe the conditions where the discrepancies can be experimentally checked, as well.

A. Experimental conditions

Table 1 presents some of the important parameters entering the choice of the experimental conditions. The values are those expected for the forthcoming São Paulo Microtron beam and photon tagging facilities [12, 13].

Table 1 - Characteristics of the experiment.

E_γ (MeV) (mean tagging energy)	3.0	5.0
N_γ^{tag} (s^{-1})	1.4×10^8	
P_γ	0.7	
ΔE_γ^{tag}/channel (MeV)	0.2	0.3
N_γ^{tag}/channel (s^{-1})	2×10^7	
N_n (cm^{-2})	9×10^{19}	
ϵ	0.013	
ΔE_p (keV)	30	7

The Bremsstrahlung beam intensity and polarization were obtained by Monte Carlo simulation [14] for an incident electron energy of 15 MeV. Photons and post-Bremsstrahlung electrons are collimated off axis. The geometry of the collimators (dimensions and positioning) was chosen in order to optimize the degree of polarization and to concentrate the photon spectral intensity in the near-threshold energy region. In this case, random coincidences, which restrict the photon beam intensity [13], arise mainly from the partial angular acceptance of the electron collimator. Signals of

reaction products from untagged photons (produced by electrons that hit the collimator) will cause random coincidences with signals from the focal plane detectors. The value of N_γ^{tag}, shown in table 1, assumes a ratio of the number of true to random coincidences $R = 1$, summed over all (seven, in this case) tagger channels. The target thickness, N_n, corresponds to a low pressure (0.5 atm), 7-cm long (along the beam direction), gaseous deuterium target. The reaction products detection system is composed of two detector planes placed at opposite sides of the target. The protons are detected by silicon strip detectors, described in ref. [15], while the neutrons are detected by plastic scintillators coupled to photomultipliers (0.025 MeV thereshold), and this will be the subject of a forthcoming publication. The absolute detection efficiency, ϵ, is typical for opposing detector pairs seeing the target at 90°. Proton energy losses in the target (ΔE_p, table 1) were calculated for 90° emission and averaged over the photon beam dimension (~ 1 cm^2).

B. Model predictions and simulation results

In this section we present the results obtained for the four different calculations performed, namely using DWF_1 or DWF_2, with or without the inclusion of final state interactions (FSI).

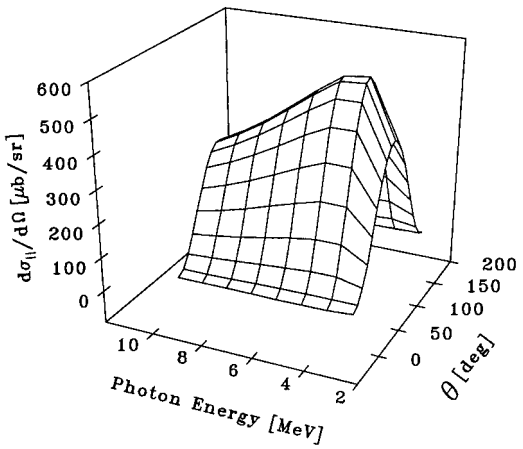

Figure 3. Differential cross sections $d\sigma_\parallel/d\Omega(E_\gamma, \theta)$, calculated with DWF for Paris potential and including FSI.

The cross sections $d\sigma_\parallel/d\Omega$ and $d\sigma_0/d\Omega$ (shown in Figs. 3 and 4 for DWF_1 with FSI) have a similar angular behavior: a maximum at $\theta = 90°$, which is characteristic of the $E1$ multipole. Calculations using other models (DWF_1 without FSI or DWF_2 with or without FSI) give results that are visually identical to those shown in Figs. 3 and 4.

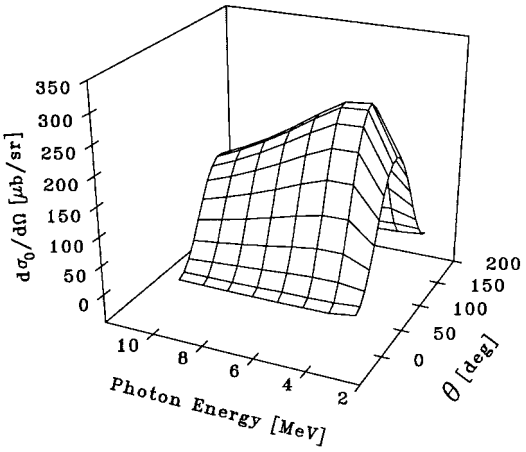

Figure 4. Differential cross sections $d\sigma_0/d\Omega(E_\gamma, \theta)$, calculated with DWF for Paris potential and including FSI.

The Σ-asymmetry is practically not sensitive to different choices of DWF, giving very close results for DWF_1 or DWF_2. It also presents very similar angular behaviors for calculations including or not FSI, as shown respectively in Figs. 5 and 6. The absolute value of the Σ-asymmetry drops for angles close to 0 and π, especially at low photon energies and in the calculations including FSI.

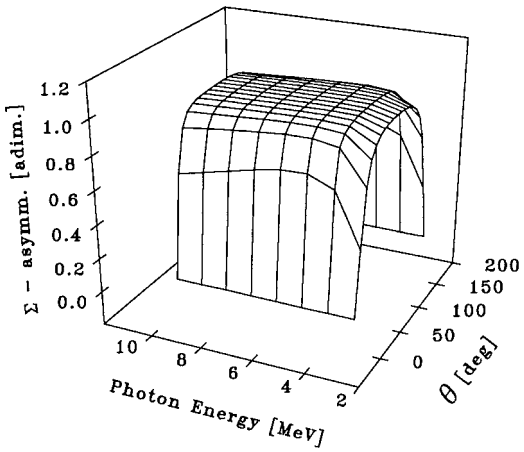

Figure 5. Σ-asymmetry, calculated with DWF for Paris potential and including FSI.

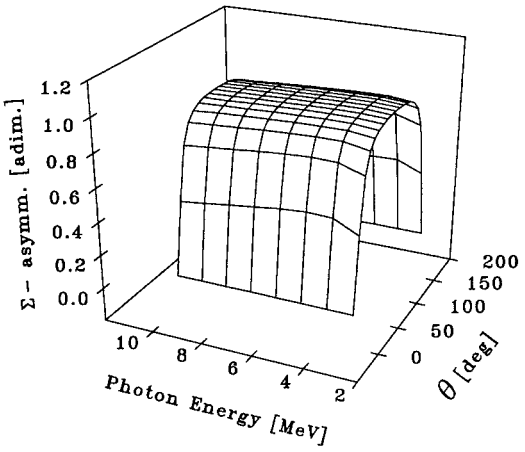

Figure 6. Σ-asymmetry, calculated with DWF for Paris potential and without FSI.

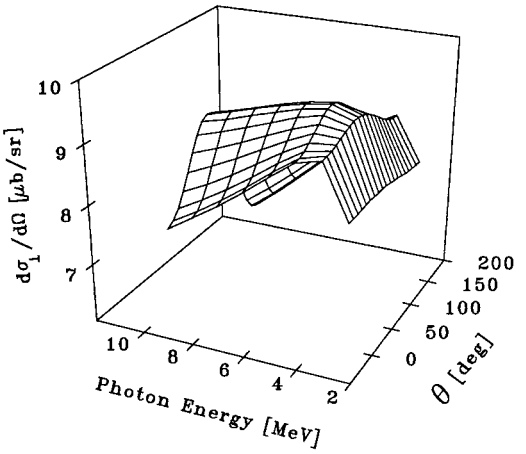

Figure 7. Differential cross sections $d\sigma_\perp/d\Omega(E_\gamma,\theta)$, calculated with DWF for Paris potential and without FSI.

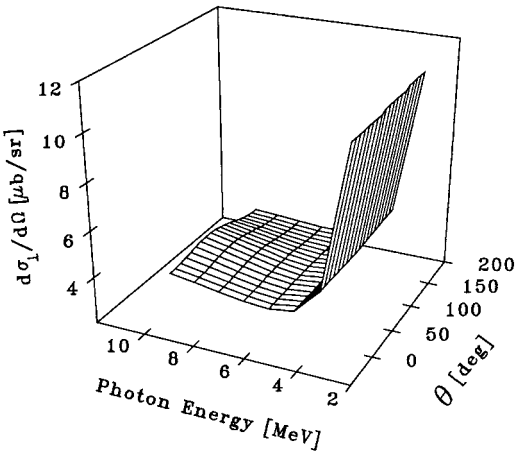

Figure 8. Differential cross sections $d\sigma_\perp/d\Omega(E_\gamma,\theta)$, calculated with DWF for Paris potential and including FSI.

As the Σ-asymmetry, the $d\sigma_\perp/d\Omega$ cross section is not sensitive to the choice of DWF, but is strongly sensitive to the inclusion of FSI. Figs. 7 and 8 show the angular and energy dependence of $d\sigma_\perp/d\Omega$ calculated using DWF_1, without and with FSI, respectively. It is interesting to note that the inclusion or not of FSI gives different results not only for the absolute value of the cross section, but it is also responsible for radical changes in the angular and energy dependence.

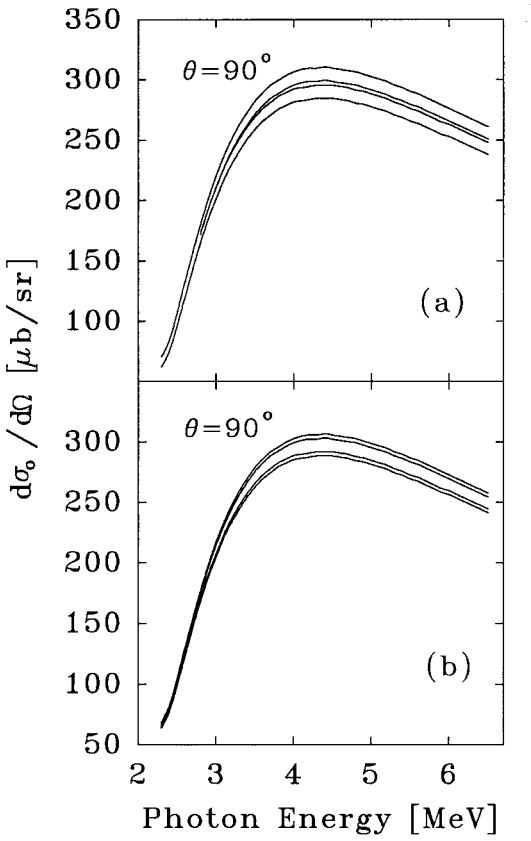

Figure 9. Differential cross sections $d\sigma_0/d\Omega(E_\gamma)$ for $\theta = 90^0$. The experimental uncertainties are shown as bands. The upper band corresponds to calculations with DWF for Paris potential (with and without the inclusion of FSI, visually the same), the lower band uses Gross potential (with and without the inclusion of FSI, visually the same). (a) corresponds to $L = 10$, and (b) to $L = 100$ ($L = 4\pi\epsilon N_n N_\gamma^{tag} t \times 10^{-30}\mathrm{sr}/\mu\mathrm{b}$, $L = 100$ corresponds to the data from table 1 and 100 h). The energy resolution for both cases is 0.2 MeV at the beginning of the range and 0.3 at the end.

Figs. 9–12 respectively show the energy dependence of $d\sigma_0/d\Omega$, $d\sigma_\parallel/d\Omega$, Σ-asymmetry and $d\sigma_\perp/d\Omega$. This form was chosen because the most convenient way of resolving the discrepancies seems to be the detailed measurement of the enery dependence of the cross sections at energies close to the threshold, at $\theta = 90°$. The ability to resolve different model calculations depends strongly on the uncertainties that can be achieved in the experiments, which, in turn, are determined by the experimental setup. The main sources of uncertainties

in the proposed experiment are the count rate statistics (due to expected low count rates) and the achievable accuracy in the determination of the degree of polarization of the photon beam. The bands (instead of curves) presented in Figs. 9–12 represent the experimental uncertainties, evaluated for the expected conditions of the São Paulo Microtron and tagger, for a typical tagger channel. The evaluation assumed the data presented in table 1 and beam times of 10, 100 or 200 h (see figure captions). The experimental uncertainties shown are only statistical. Possible systematic errors arising from the absolute values of the cross sections or the degree of polarization, were not considered. The energy resolution is about 0.2 MeV in the beginning of the range and about 0.3 MeV at the end. It corresponds to the width of the tagger channel.

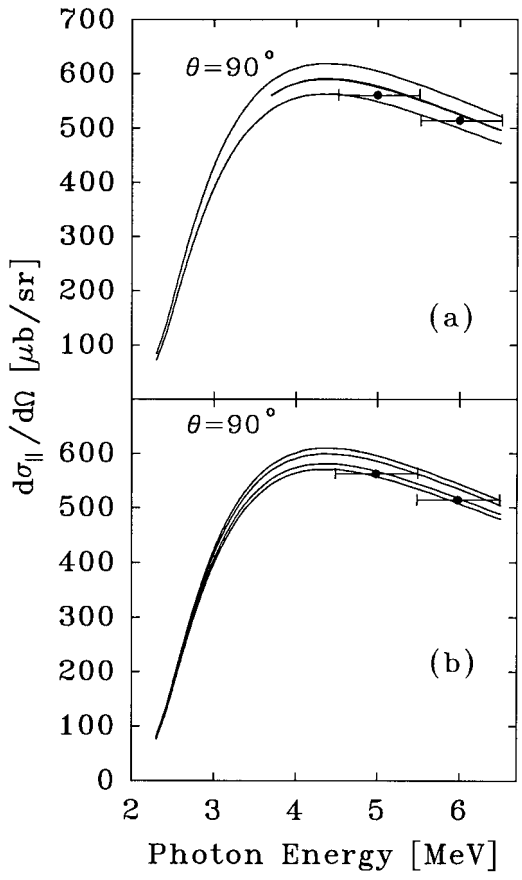

Figure 10. Differential cross sections $d\sigma_{\parallel}/d\Omega(E_\gamma)$ for $\theta = 90^0$. All designations are the same as in Fig. 9. The uncertainties of the experimental data are only statistical.

As it can be seen from Figs. 9 and 10, $d\sigma_{0,\parallel}/d\Omega$, in the energy range 2.5–6.0 MeV, is sensitive to the DWF choice (the bands are separated) but not to FSI effects. On the other hand, Σ and $d\sigma_{\perp}/d\Omega$ (shown in Figs. 11 and 12) are not sensitive to the choice of DWF, but pinpoint FSI effects. From Figs. 9–12 one can also select the energy ranges where the bands do not overlap, which should be favoured in the measurements.

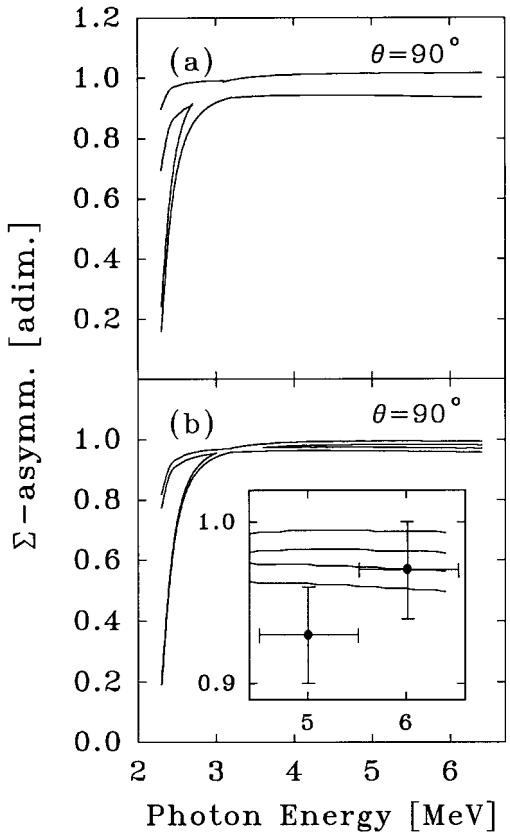

Figure 11. Σ-asymmetry for $\theta = 90^0$ versus photon energy, calculated with DWF for Paris and Gross potentials (not distinguished) with FSI (lower band) and without FSI (upper band). Bands in (a) correspond to $L = 10$ and in (b) to $L = 200$ (see caption of Fig. 9). The uncertainties of the experimental data are only statistical.

Figs. 10–12 also present some preliminary data, obtained with photons from channeling and similar equipment (gaseous target and silicon detectors). The experimental details are presented in ref. [16]. It can be seen from Fig. 10 that the experimental uncertainties (about 1%) would be enough to distinguish between Paris and Gross potentials if a better energy resolution is available. On the other hand, the data for Σ and $d\sigma_{\perp}/d\Omega$ (Figs.11 and 12), even though favouring the calculation including FSI, could certainly be improved with better statistics and energy resolution. Moreover, since the photons were obtained by the channeling process, the degree of the polarization of the beam is subject to uncertainties and, as shown below, this strongly affects the confidence on the data.

Equations (7) and (9) define how sensitive is the analysis to systematic errors in the cross sections and degree of polarization of the photon beam. A 1% change in $d\sigma_0/d\Omega$ or P_γ shifts the bands of $d\sigma_\parallel/d\Omega$ of 1% or 0.5% respectively, in the range where $\Sigma \approx 0.98$ (see Fig. 11), which are much smaller than the 5% difference between the curves. The situation with $\sigma_\perp/d\Omega$ is quite diffeferent. The same 1% change in $d\sigma_0/d\Omega$ or P_γ shifts the bands of $d\sigma_\perp/d\Omega$ of 1% and 100% respectively, which should be compared with the $\sim 100\%$ difference between both theoretical predictions. So, in order to be able to distiguish between the different calculations, the systematic errors in $d\sigma_0/d\Omega$ and P_γ must be within 5% and 1%, respectively.

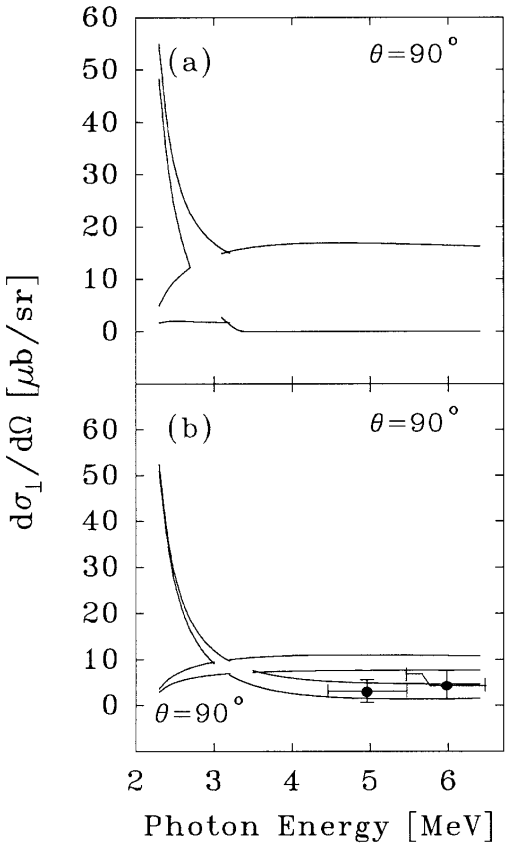

Figure 12. Differential cross sections $d\sigma_\perp/d\Omega(E_\gamma)$ for $\theta = 90^0$ versus photon energy, calculated with DWF for Paris and Gross potentials (not distinguished) with FSI (upper band, below 3 MeV) and without FSI (lower band, below 3 MeV). Bands in (a) correspond to $L = 10$ and in (b) to $L = 200$ (see caption of Fig. 9). The uncertainties of the experimental data are only statistical.

V. Conclusions

This work shows that, in the near-threshold energy region, where discrepancies between different models do exist, there are no experimental data with enough accuracy to resolve those discrepancies. Angular distributions of differential cross sections, which contain information about the multipolarity of the transitions, are also completely absent.

The considerations presented previously show that, within the experimental conditions that will be available at the São Paulo Microtron and tagging facilities, it will be possible to assess the assumptions of the relativistic gauge-invariant model of nuclear photodisintegration and, in particular, to differentiate between the deuteron wave functions based on Paris or Gross potentials by measuring $d\sigma_0/d\Omega$ or $d\sigma_\parallel/d\Omega$; also, the inclusion or not of final state interaction effects can be resolved by the measurement of $d\sigma_\perp/d\Omega$ or the Σ-asymmetry.

The analysis presented here can be considered as a study of (*i*) the necessary conditions to be achieved by the experimental equipment and acquisition system to be used in the measurement and (*ii*) the necessary accuracy to be achieved in the determination of the absolute value of the cross section $d\sigma_0/d\Omega$ (better than 5%) and the degree of polarization of the photon beam (better than 1%).

Acknowledgments

One of us (V.P.L.) acknowledges support by Conselho Nacional de Desenvolvimento Científico e Tecnológico, CNPq, under grant number 300961/93–6.

References

[1] H. Arenhövel and M. Sanzone, *Photodisintegration of the deuteron*, report MKPH-T-90-9, Mainz, 1990.

[2] D.A. Varshalovich, A.N. Moskalev and V.K. Khersonskij, *Quantum Theory of Angular Momentum*, World Scientific, Singapore, 1988.

[3] A.I. Akhiezer and V.B. Berestetskii, *Quantum Electrodynamics*, Interscience Publishers, New York, 1965.

[4] V.P. Likhachev, M.N. Martins, J.D.T. Arruda-Neto, C.C. Bueno, M. Damy de S. Santos, I.G. Evseev, J.A.C. Gonçalves, O.A.M. Helene, S.A. Paschuk and H.R. Schelin, *Geometrical parameters of a detection system: a Monte Carlo approach*, Nucl. Instrum. Meth. A (submitted).

[5] S.I. Nagornyi, Yu.A. Kasatkin and V.A. Zolenko, Phys. Lett. B **316**, 231 (1993).

[6] S.I. Nagornyi, Yu.A. Kasatkin and V.A. Zolenko, Phys. Atomic Nuclei **57**, 940 (1994).

[7] S.I. Nagornyi, Yu.A. Kasatkin, E.V. Inopin and I.K. Kirichenko, Sov. J. Nucl. Phys. **44**, 760 (1986).

[8] A.A. Zayats, V.A. Zolenko, Yu.A. Kasatkin and S.I. Nagornyi, Sov. J. Nucl. Phys. **55**, 301 (1992).

[9] J. Haidenbauer and W. Plessas, Phys. Rev. C **30**, 1822 (1984).

[10] M. Lacombe, B. Loiseau, R. Vinh-Mau, J. Côté, P. Pires and R. de Tourreil, Phys. Lett. B **101**, 139 (1981).

[11] W.W. Buck and F. Gross, Phys. Rev. D **20**, 2361 (1979).

[12] J. Takahashi, Y. Miyao, M.N. Martins, J.M. Machado, A.A. Malafronte, J.C.A. Alcon, J.M. Junior and A. Bonini, *The IFUSP racetrack microtron*, 3rd European Particle Accelerator Conference, Berlin, 1992.

[13] J.-O. Adler, B.-E. Andersson, K.I. Blomqvist, B. Forkman, K. Hansen, L. Isaksson, K. Lindgren, D. Nilsson, A. Sandell, B. Schröder and K. Ziakas, Nucl. Instrum. and Methods A **294**, 15 (1990) and R. Guarino, V.P. Likhachev and M.N. Martins, Pre-print IFUSP/P-1149 (1995).

[14] M.N.Martins, V.P. Likhachev, J.D.T. Arruda-Neto, R. Guarino and F. Gerab, *Tagged bremsstrahlung polarization: a Monte Carlo approach*, Nucl. Instrum. Meth. A (submitted).

[15] V.P. Likhachev, J.F. Dias, M.L. Yoneama, M.N. Martins, J.D.T. Arruda-Neto, C.C. Bueno, V. Perevertailo and O. Florov, *Silicon strip detectors for fission*, Nucl. Instrum. Meth. A **376**, 455 (1996).

[16] A.Yu. Buki, Yu.V. Vladimirov, V.V. Denyak, I.G. Evseev, A.A. Zayats, Yu.A. Kasatkin, V.I. Kasilov, I.K. Kirichenko, N.I. Lapin, V.P. Likhacher, S.I. Nagornyi, S.A. Pashchuk, E.V. Pegushin, V.M. Sanin, V.M. Khvastunov and S.F. Shcherbak, Sov. J. Nucl. Phys. **51**, 1208 (1990).